GA–A25592

STABILITY AND DYNAMICS OF THE EDGE PEDESTAL IN THE LOW COLLISIONALITY REGIME: PHYSICS MECHANISMS FOR STEADY-STATE ELM-FREE OPERATION

by
P.B. SNYDER, K.H. BURRELL, H.R. WILSON, M.S. CHU,
M.E. FENSTERMACHER, A.W. LEONARD, T.H. OSBORNE,
M. UMANSKY, W.P. WEST, X.Q. XU

APRIL 2006

GENERAL ATOMICS

DISCLAIMER

GA–A25592

STABILITY AND DYNAMICS OF THE EDGE PEDESTAL IN THE LOW COLLISIONALITY REGIME: PHYSICS MECHANISMS FOR STEADY-STATE ELM-FREE OPERATION

by
P.B. SNYDER, K.H. BURRELL, H.R. WILSON,* M.S. CHU,
M.E. FENSTERMACHER,† A.W. LEONARD, T.H. OSBORNE,
M. UMANSKY,† W.P. WEST, X.Q. XU†

This is a preprint of a paper to be presented at the 21st IAEA Fusion Energy Conference, October 16-21, 2006, in Chengdu, China, and to be published in the Proceedings.

*Department of Physics, University of York, Heslington, York, UK
†Lawrence Livermore National Laboratory, Livermore, California

Work supported by
the U.S. Department of Energy under
DE-FG02-95ER54309, DE-FC02-04ER54698
and W-7405-ENG-48

GENERAL ATOMICS PROJECT 03726
APRIL 2006

GENERAL ATOMICS

ABSTRACT

Understanding the physics of the edge pedestal and edge localized modes (ELMs) is of great importance for ITER and the optimization of the tokamak concept. The peeling-ballooning model has quantitatively explained many observations, including ELM onset and pedestal constraints, in the standard H-mode regime. The ELITE code has been developed to efficiently evaluate peeling-ballooning stability for comparison to observation and predictions for future devices. We briefly present recent progress in the peeling-ballooning model, including studies of the apparent power dependence of the pedestal, and studies of the impact of sheared toroidal flow. Nonlinear 3D simulations of ELM dynamics using the BOUT code are also described, leading to an emerging understanding of the physics of the onset and dynamics of ELMs in the standard intermediate to high collisionality regime. Recently, highly promising low collisionality regimes without ELMs have been discovered, including the quiescent H-mode (QH) and resonant magnetic perturbation (RMP) regimes. We present recent observations of the density, shape and rotation dependence of QH discharges, and studies of the peeling-ballooning stability in this regime. We propose a model of the QH-mode in which the observed edge harmonic oscillation (EHO) is a saturated kink/peeling mode which is destabilized by current and rotation, and drives significant transport, allowing a near steady-state edge plasma. The model quantitatively predicts the observed density dependence, and qualitatively predicts observed mode structure, rotation dependence, and outer gap dependence. Low density RMP discharges are found to operate in a similar regime, but with the EHO replaced by an applied magnetic perturbation.

1. INTRODUCTION

Edge localized modes (ELMs) limit tokamak performance both directly, via large transient heat loads to material surfaces, and indirectly, through constraints placed on the edge pedestal height which strongly impact global confinement. Maximizing the pedestal height (p_{ped}) while maintaining acceptable ELM behavior is a key issue for optimizing tokamak performance and is of great importance for the success of ITER.

Progress in the peeling-ballooning model [1-3] has led to an emerging understanding of the physics of the onset and dynamics of ELMs in the standard moderate to high collisionality pedestal regime. However, the pedestal physics of low collisionality regimes, such as quiescent H-mode (QH) and resonant magnetic perturbation (RMP) has been less understood. We summarize the peeling-ballooning model and its implementation and validation in Section 1.1, then highlight recent progress in exploring apparent pedestal power dependence (Section 1.2), the role of toroidal flow (Section 1.3), and nonlinear ELM dynamics studied via large scale 3D simulations (Section 1.4). In Section 2, we focus on pedestal physics in the low collisionality regime, discussing the role of collisionality, QH-mode observations, and a model for the QH-mode and its accompanying edge harmonic oscillation (EHO). Finally, we briefly discuss the RMP regime.

1.1. THE PEELING-BALLOONING MODEL AND ITS VALIDATION

The outer ("pedestal") region of high performance ("H-mode") tokamak plasmas is characterized by a sharp pressure gradient and consequent large bootstrap current, as shown in Fig. 1(a). The peeling-ballooning model posits that the free energy in the large pressure gradients and current drives coupled peeling-ballooning modes that constrain the maximum pressure at the top of the pedestal region ("pedestal height") and drive ELMs. Peeling-ballooning theory was first developed in the local high toroidal mode number (n) limit [1], and later extended to incorporate intermediate-n and non-locality [4,2]. An efficient 2D numerical code, ELITE [4,2], has been developed to study these nonlocal, finite-n peeling, ballooning, and coupled peeling-ballooning modes. Other 2D MHD codes such as MISHKA [5] are also used for this purpose, and ELITE has been successfully benchmarked against MISHKA, as well as GATO, CASTOR, MARG2D and BAL-MSC. A schematic diagram of peeling-ballooning stability boundaries is shown in Fig. 1(b). While the precise stability boundaries are non-local, and depend on details of the pressure and current profiles, it is useful for simplicity to present results as a function of local quantities, here the maximum pressure gradient in the pedestal region, and a characteristic value of the edge current. For typical H-mode edge parameters, the limiting instability is usually an intermediate-n ($n \sim 3-30$) coupled peeling-ballooning mode, though pure ballooning modes can be limiting at high collisionality, and pure kink/peeling modes at low collisionality (Section 2). The very

strong effect of shape on the stability boundaries can be seen in Fig. 1(b). A 3D rendering of the mode structure of an $n = 18$ peeling-ballooning mode in DIII-D is shown in Fig. 1(c).

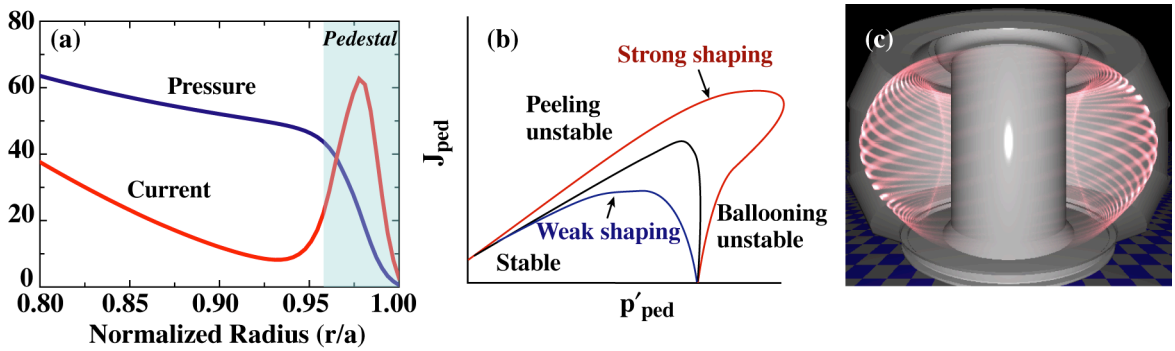

Fig. 1. (a) Typical pressure and current profiles in the H-mode edge region. (b) Schematic diagram of the peeling-ballooning stability limit for different shaped discharges as a function of edge current and pressure gradient. (c) Mode structure of an $n = 18$ peeling-ballooning mode calculated by ELITE.

The inclusion of finite-n, nonlocal physics via the availability of efficient 2D codes has led to numerous successful comparisons of the model to experiment. These include comparisons of calculated variation of edge stability with parameters such as shape and density [2], and direct comparisons of the stability of particular discharges with ELM observations and pedestal constraints in those discharges [2,6-8]. Over 100 discharges have now been studied with ELITE, and it is generally found that the discharges are stable well before ELMs occur, and then approach the peeling-stability boundary just before ELMs are observed. An example of such a study in DIII-D is shown in Fig. 2(a), where the X marks the location in parameter space of the discharge just before an ELM, and the stability boundary is calculated by varying the pressure and current profiles around their measured values and calculating $n = 5$–30 stability with ELITE. A finite growth rate threshold is typically used to account for diamagnetic stabilization. The good agreement in these comparisons, which have no free parameters, across dozens of discharges on several tokamaks strongly suggests that the MHD peeling-ballooning model, accounting for diamagnetic stabilization via a growth rate threshold, is able to successfully explain the onset of high power (Type I) ELMs and the associated pedestal constraints.

1.2. POWER DEPENDENCE OF THE PEDESTAL

A key physics issue for projecting performance of future tokamaks is the dependence of pedestal height on input power. It has been observed in database studies that pedestal height typically increases weakly with input power. Part of this observed correlation is due to the inclusion of “soft” regimes such as EDA and Type III ELMs in the database. However, even when restricted to Type I and Type II ELM regimes, some power dependence remains.

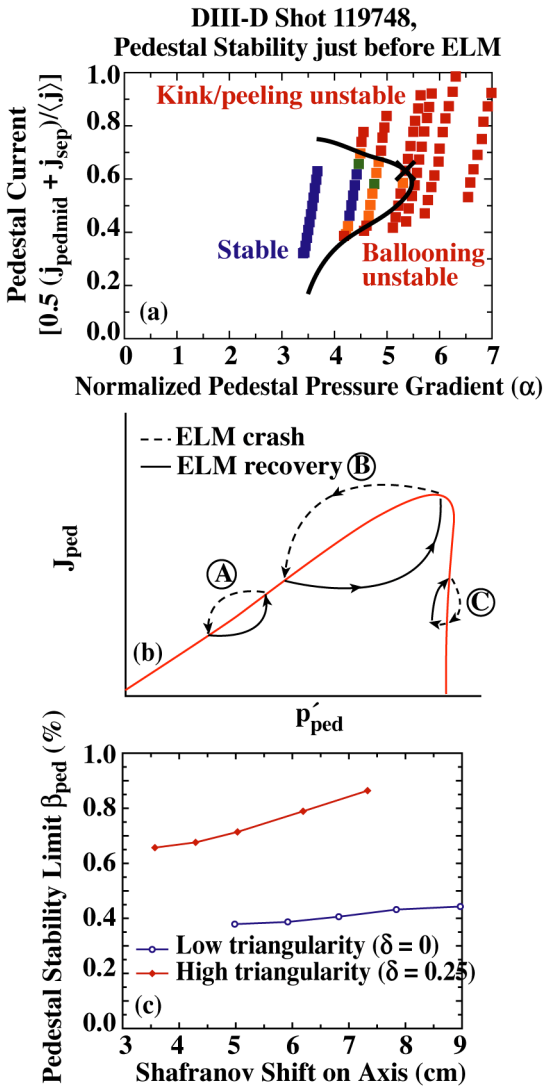

Fig. 2. (a) Stability diagram for a DIII-D discharge, showing the discharge (X) is approaching the stability bound just before an ELM is observed. (b) Schematic of various possible ELM crash and recovery cycles. (c) Dependence of the pedestal stability boundary on the Shafranov shift for low and high triangularity cases.

This result may initially appear difficult to understand in light of the peeling-ballooning model, which has no explicit power dependence. However, several possible mechanisms exist, some of which have been identified in observations. (1) Kink/peeling constrained: several types of ELM crash and recovery cycle are possible, as illustrated in Fig. 2(b). In the cycle labeled "A" a largely current-driven kink/peeling mode causes the ELM. In this case the pedestal is limited by current rather than pressure, and increasing the input power will allow an increase in the pressure gradient and resulting pedestal height (the ELM recovery trajectory will extend to a higher value in pressure before the bootstrap current has time to

evolve and drive the ELM). This mechanism is observed in a power scan in JET in Ref. 8. (2) Shafranov shift dependence: we find that in many cases, particularly with strong shaping, that the maximum stable pedestal height increases with Shafranov shift [Fig. 2(c)]. The Shafranov shift is proportional to global β_{pol}, and thus increases with heating power, as core profiles steepen. This can lead to a virtuous cycle, in which increasing power increases core gradients, leading to larger Shafranov shift and allowing a higher pedestal. The higher pedestal in turn allows yet higher core pressure, due to profile stiffness effects, and yet higher β_{pol}, and the cycle continues. The very weak dependence in pedestal height with power (and β_{pol}) at weak shaping, and the stronger dependence at strong shaping predicted in Fig. 2(c) is in good agreement with DIII-D observations. (3) Increasing second stability: as can be seen in Fig. 1(b), the stability boundary at the upper right of the diagram (the so-called "second stability" region when it extends out beyond the infinite-n ballooning limit) is particularly sensitive. Small changes in discharge or profile shape can strongly impact the stability boundary in this region. We have found in studies on DIII-D that increasing power can alter profiles in such a way that the peeling and ballooning modes become decoupled and the stability boundary moves to higher pressure [resembling a change from black to red curves in Fig. 1(b)]. (4) Pedestal width: a change in profile shape with power that leads to an increase in the width of the sharp gradient region will generally increase the stability constraint on the pedestal height. We note this increase is not linear, due to the non-locality of the stability constraint (typically the maximum stable pedestal height scales roughly as the width to the 0.7 power). The physics setting the pedestal width remains poorly understood, but there are indications of some correlation with input power.

1.3. IMPACT OF TOROIDAL FLOW

Sheared toroidal flow has been incorporated into the ELITE formalism and code, and successfully benchmarked against the low-n MARS code [Fig. 3(a)]. As expected from infinite-n theory, we find that sheared flow is strongly stabilizing to very high-n modes. However, at longer wavelength this effect weakens, and low-n modes can be destabilized by flow shear, as shown in Fig. 3(b) for a ballooning unstable case with constant flow shear. The result is that the overall (all n) critical gradient does not generally change substantially with flow shear, but the most unstable mode moves to longer wavelength. The flow does have a significant impact on the mode structure and the mode evolution. Notably, we find via fast rotation measurements on DIII-D that the initially strongly sheared flow in the pedestal region collapses during an ELM to approximately a constant flow at the most unstable peeling-ballooning mode's eigenfrequency. This collapse weakens the H-mode barrier and is expected to lead to substantial transport, contributing to the ELM losses of heat and particles.

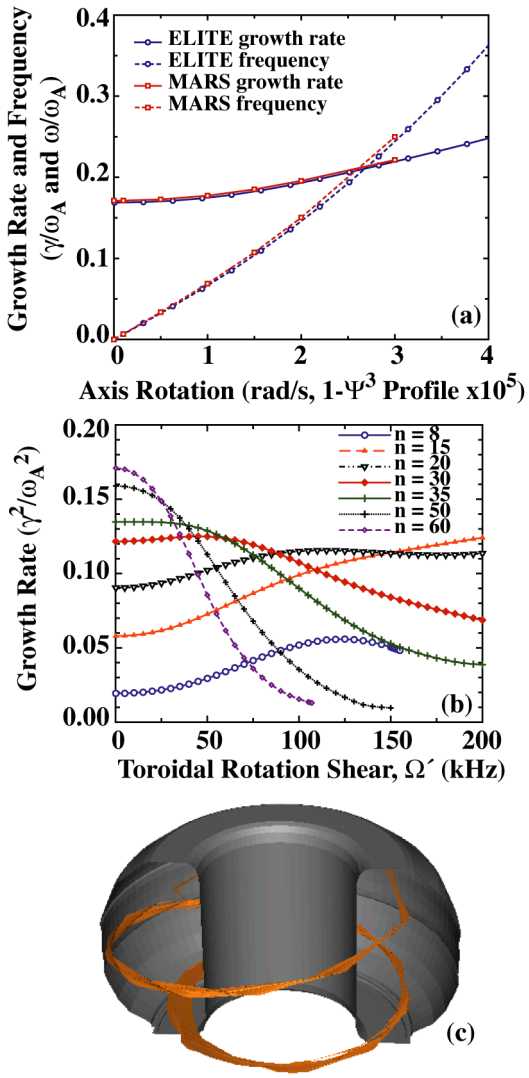

Fig. 3. (a) Comparison of growth rate and frequency calculated by ELITE and MARS for an $n = 8$ mode with cubic toroidal flow profile. (b) Variation in growth rate with flow shear for a ballooning mode, showing strong stabilization at high n, and destabilization at lower n. (c) Filament of plasma from a nonlinear ELM simulation with BOUT propagates rapidly outward toward the vessel wall.

1.4. NONLINEAR 3D SIMULATIONS OF ELM DYNAMICS

While linear calculations are useful for understanding ELM onset conditions and pedestal constraints, nonlinear simulations are needed to understand ELM associated particle and heat losses and their deposition on material surfaces. We have conducted a series of realistic 3D nonlinear simulations of ELMs using the BOUT code. BOUT [9] is a 3D electromagnetic, reduced-Braginskii simulation code which incorporates full non-local geometry including the pedestal region and scrapeoff layer. It accounts for both the large-scale MHD drives and

smaller scale diamagnetic terms in the collisional limit. A series of nonlinear ELM simulations with BOUT and comparison to observation is presented in Ref. 3. In the early phase of these simulations, the onset conditions for an ELM is found to be similar to those calculated with ELITE (but modified slightly due to diamagnetic effects), and the mode structure is typical of a linear peeling-ballooning mode [as in Fig. 1(c)]. Later in the simulation, an explosive burst of one or many filaments propagates radially from the pedestal, through the scrape-off-layer and toward the wall. The density perturbation at a late time for a single filament case is shown in Fig. 3(c). The nonlinear evolution of the filaments is similar to that from semi-analytic ballooning theory [10]. The filamentary structure, wavelength, and presence of one or many filaments are all in good agreement with direct ELM observations, and the radial propagation velocity of the simulations is in qualitative agreement [3].

Combining the results of nonlinear ELM simulations with the collapse of edge flow shear discussed in the previous section, we have developed a two pronged model for the energy and particle losses associated with ELMs. (1) Conduits: the filaments remain connected at the top and bottom to the hot core plasma, fast local diffusion and secondary instabilities along the outer portion of the filament allow fast parallel losses of heat and particles. (2) Barrier collapse: the growth and propagation of the mode collapses the flow shear in the edge region and weakens or destroys the edge transport barrier, resulting in a temporary return of L-mode transport until the barrier recovers.

2. PEDESTAL PHYSICS IN THE LOW COLLISIONALITY REGIME

As described in the previous sections, there is an emerging understanding of the physics of ELMs and pedestal constraints in the usual moderate to high collisionality regime. Recently, highly promising low-collisionality regimes have been discovered, in which a robust, steady H-mode with high pedestal is achieved in the absence of ELMs. These include the QH regime, observed on DIII-D, ASDEX-U, JT-60U and JET at ITER relevant β and ν^* values, and recently extended to long duration and completely ELM-free operation [11]; as well as low-density ELM-free discharges in which ELMs are suppressed via an externally applied RMP [12,13]. The focus of this section is to understand the pedestal physics in these promising low collisionality, ELM-free regimes.

The effect of collisionality is very important in the peeling-ballooning model [Fig. 4(a)]. The bootstrap current, which typically dominates in the edge region, is roughly proportional to the pressure gradient, but is reduced by collisions. Hence as the collisionality is reduced, more current is produced at a given pressure gradient. At a given pressure, collisionality is proportional to the cube of the density. Thus, at high density, the pedestal follows a parameter trajectory as given by the magenta arrow in Fig. 4(a) and encounters the ballooning stability boundary, while at low density (green trajectory) it encounters the relatively low-n kink/peeling boundary (low n instability is marked with red squares). The maximum density at which the pedestal is low-n limited depends strongly on shape (here triangularity), as seen by comparing Fig. 4(a) and 4(b). We posit that a necessary condition for QH-mode operation is that the plasma must be in this low-n kink/peeling limited regime. This leads to a prediction of the maximum density possible in QH-mode of $\sim 4\times10^{19}$ m^{-3} in the DIII-D high triangularity case, and $\sim 1.5-2\times10^{19}$ m^{-3} in the low triangularity case. These values are in good agreement with the observed maximum QH densities in weakly and strongly shaped discharges [11], and a wide range of QH discharges studied to date confirm that QH operation occurs near the kink/peeling stability boundary. We apply the same technique to predict the pedestal density required for QH operation in the ITER base case and find [Fig. 4(c)] a value $\lesssim 4\times10^{19}$ m^{-3} is required. This is low compared to the design average density of $\sim 10^{20}$ m^{-3}, but could be achieved either by density peaking or by reducing the design density. Operating ITER at low pedestal density has divertor implications which should be studied.

During the 2006 campaign on DIII-D, a new high triangularity near double-null QH-mode shape was introduced. This shape was predicted to have a higher QH-mode density limit than previous shapes, and indeed record QH-mode densities were achieved, with Greenwald fractions above 0.5. An example stability diagram for one of these discharges is shown in Fig. 5(a). The discharge is up against the kink/peeling stability limit, as expected in

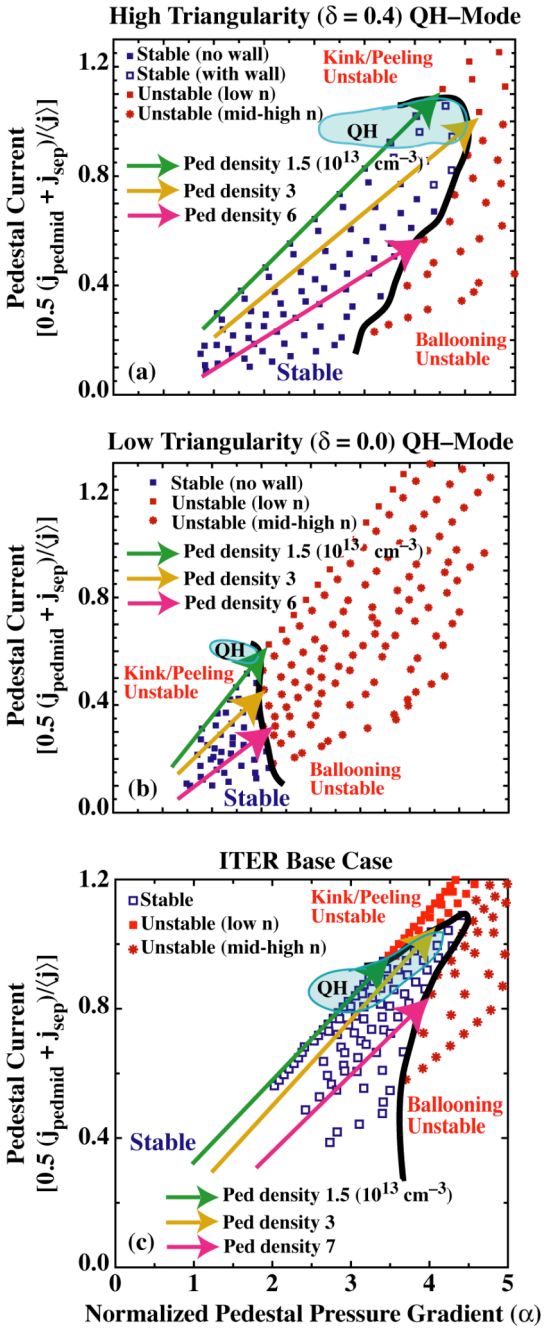

Fig. 4. Peeling-ballooning stability diagram for a model DIII-D QH discharge showing the effect of density (collisionality) on the discharge trajectory, and indicating the density required to access the proposed QH region (shaded blue) for (a) high and (b) low triangularity discharges. (c) The same diagram for ITER, indicating pedestal density required for QH-mode access.

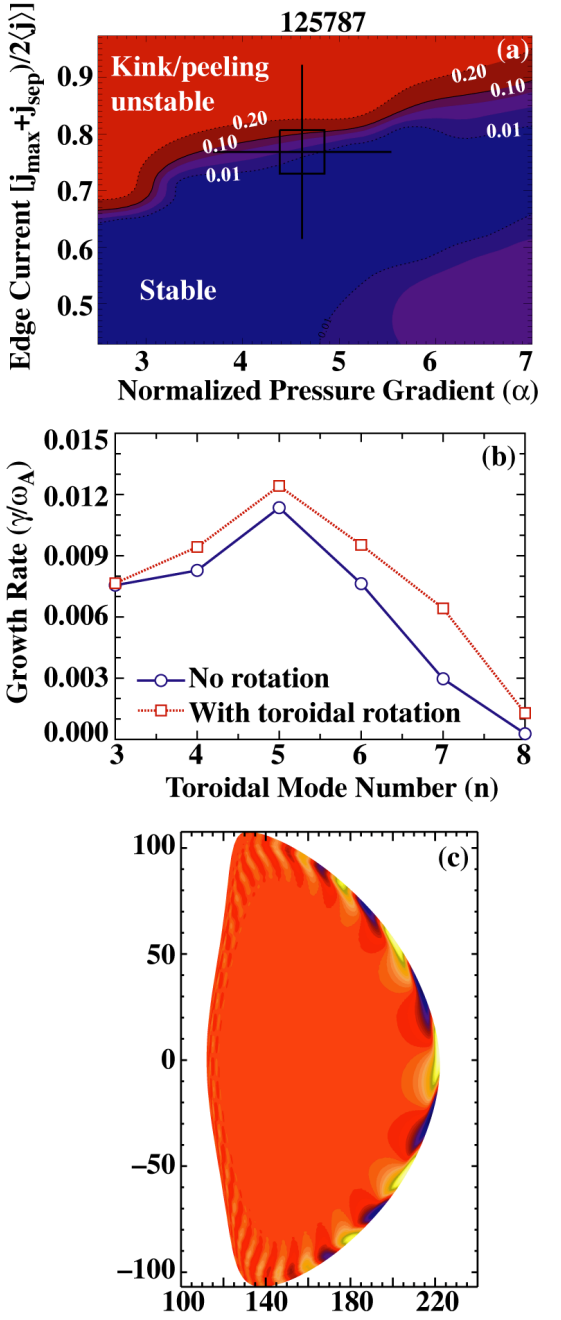

Fig. 5. (a) Peeling-ballooning stability diagram for DIII-D QH-mode shot 125787, showing QH-mode operation (crosshair) occurs near the kink/peeling stability boundary. (b) Corresponding growth rate spectrum, showing $n = 5$ is the most unstable mode, and that rotation is de-stabilizing. (c) Mode structure of the $n = 5$ mode with rotation.

QH-mode, and there is significant margin for increasing the pedestal density (4×10^{19} m^{-3}) while remaining in the low-n kink/peeling limited regime. Values up to 6×10^{19} m^{-3} are achieved in similar QH discharges with the same shape. The calculated mode spectrum shows a peak at $n=5$ [Fig. 5(b)] and indeed an $n=5$ signal is observed. The unstable mode structure calculated by ELITE is shown in Fig. 5(c). While this $n=5$ mode has too fine a structure to allow direct comparison to magnetics measurements, comparisons using an $n=1$ dominated case find good qualitative agreement between the predicted mode structure and the observed EHO.

Toroidal flow also plays an important role in the physics of QH-mode. Because the limiting modes are low-n, they couple more strongly to the conducting wall, leading to a region [open symbols, Fig. 4(a)] of wall stabilization where a slow growing "edge localized resistive wall mode" (ELRWM) is unstable in the absence of rotation. Strong edge region rotation in the QH-mode edge stabilizes this ELRWM allowing operation up to approximately the ideal wall kink/peeling boundary. Also, while toroidal flow shear stabilizes high-n ballooning modes [Fig. 3(b)], it is actually destabilizing to the low-n modes which are limiting in QH-mode, as shown in Fig. 5(b). This impacts the dynamic evolution of the mode. As the mode grows up, it damps the sheared flow in the edge region (Section 1.3). In a typical ELM case, this damping of the sheared flow further drives the instability leading to accelerating mode growth. On the contrary, in the QH-mode case, damping rotation actually stabilizes the mode, aiding its saturation. Mode coupling to the wall provides a further mechanism for rotation damping and mode saturation. Finally, because the mode itself has an eigenfrequency characteristic of the plasma rotation near the top of the pedestal, the flow shear in that region determines the rate at which the plasma rotates relative to various parts of the mode, and some types of transport mechanisms will be proportional to this rate.

The role of rotation in QH-mode has been studied in a recent series of experiments on DIII-D. These experiments begin with three neutral beams driving rotation in the counter-current direction, and then at $t=3$ s, some fraction of the counter-beams are replaced by beams in the opposite direction, reducing rotation. The results are shown in Fig. 6. When the fraction of co-beams is less than ~1/4, the pedestal rotation is reduced, but remains above 30 km/s in the counter direction, and the discharge remains quiescent with relatively constant density. When the fraction of co-beams is increased further, the pedestal rotation drops down to ~20 km/s, the pedestal density rises, and after 400-500 ms, ELMs return. Further experiments varying the size of the outer gap find that at very large outer gap, where mode coupling to the wall is weak, ELMs return. These results confirm the expected role of rotation and wall coupling, but further analysis is required to distinguish the quantitative importance of various mechanisms.

In summary, we propose a model of the QH-mode in which the EHO, a typically n~1-5 mode observed in most QH plasmas, is a saturated kink/peeling mode, which is destabilized

by edge by edge current and rotation. As its eigenmode grows to large amplitude, it creates significant magnetic perturbations which allow particle and current transport across the field. In addition, the large amplitude mode applies a drag on rotation, allowing the nonlinear mode to damp its drive and saturate at finite amplitude (rather than growing explosively like an ELM). This allows a steady state in all important transport channels and leads to a steady quiescent edge. Necessary conditions for QH density have been predicted and agree quantitatively with experiment. Rotation and wall separation requirements as well as EHO mode structure agree qualitatively with observations.

Suppression of ELMs via an imposed RMP [12-13] occurs in a similar regime. Here we propose that the RMP plays a similar role to the EHO in QH-mode, driving substantial transport and allowing an approximately steady state edge. In this case, the RMP is externally applied with controlled intensity, such that the edge parameters can be held either close to, or well below the peeling-ballooning stability boundary. We have studied several RMP discharges and consistently found that in ELM-free RMP operation, the discharge is stable to peeling-ballooning modes, while when ELMs return, the discharge is unstable to intermediate-n modes just before ELMs are observed (Fig. 7).

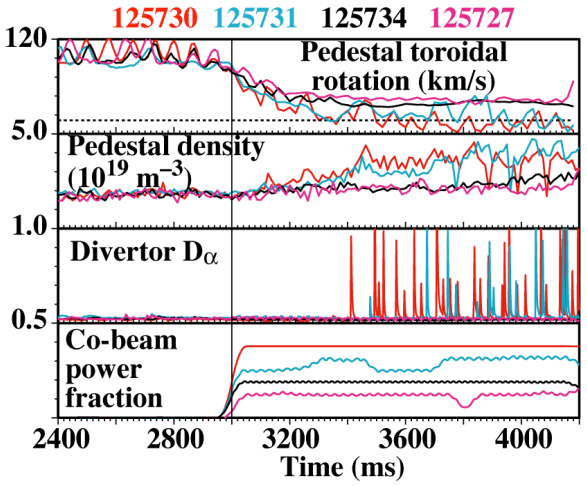

Fig. 6. A series of DIII-D QH-mode discharges in which rotation is reduced until the QH rotation boundary is found. Discharges with less than 1/4 co-beam power fraction remain quiescent (125734 and 125729) while those with larger co-beam fractions develop ELMs.

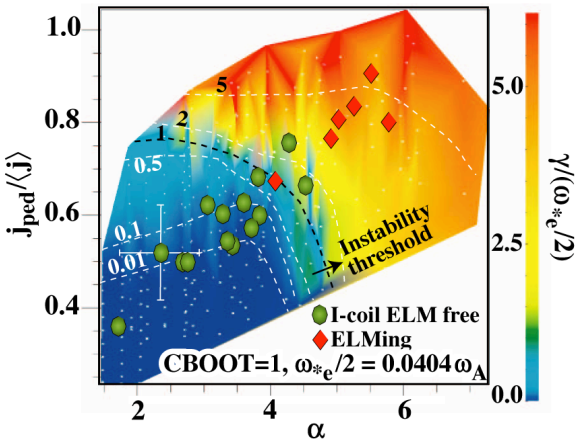

Fig. 7. Peeling-ballooning stability diagram for a series of RMP ELM-free discharges (green circles) compared with phases of similar discharges with ELMs (red diamonds).

REFERENCES

[1] CONNOR, J.W., et al., Phys. Plasmas **5** (1998) 2687.

[2] SNYDER, P.B., et al., Phys. Plasmas **9** (2002) 2037; Nucl. Fusion **44** (2004) 320.

[3] SNYDER, P.B., et al., Phys. Plasmas **12** (2005) 056115**.**

[4] WILSON, H.R., et al., Phys. Plasmas **9** (2002) 1277.

[5] HUYSMANS, G.T.A., et al., Phys. Plasmas **8** (2001) 4292.

[6] MOSSESSIAN, D.A., et al., Phys. Plasmas **10** (2003) 1720; KIRK, A., et al. Plasma Phys. Control. Fusion **46** (2004) 551; SAARELMA, S., et al., Plasma Phys. Control. Fusion **47** (2005) 713.

[7] LEONARD, A.W., this conference

[8] ONJUN, T., et al., Phys. Plasmas **11**, (2004) 1469.

[9] XU, X.Q., et al., New J. of Physics **4** (2002) 53; Nucl. Fusion **42** (2002) 21.

[10] WILSON, H.R., and COWLEY, S.C., Phys. Rev. Lett. **92** (2004) 175006.

[11] BURRELL, K.H., et al., Phys. Plasmas **12** (2005) 056121; WEST, W.P., et al., Nucl. Fusion **45** (2005) 1708.

[12] BURRELL, K.H., et al., Plasma Phys. Control. Fusion **47** (2005) B37-52.

[13] EVANS, T.E., et al., Nature Physics **2** (2006) 419.

ACKNOWLEDGMENT

This work supported by the U.S. Department of Energy under DE-FG02-95ER54309, DE-FC02-04ER54698, W-7405-ENG-48 and in part by the UK EPSRC and Euratom. We gratefully acknowledge contributions from the DIII-D Team.